Competition between electroconvection and Fréedericksz distortions in nematic liquid crystals with slightly positive dielectric anisotropy

B. Dressel and W. Pesch
Physikalisches Institut der Universität Bayreuth, D-95440 Bayreuth, Germany
(Received 3 December 2002; published 26 March 2003)

Planar electroconvection in nematic liquid crystals with positive dielectric anisotropy is theoretically studied in the nonlinear regime. The system is characterized by a competition between the nonequilibrium electroconvection instability and the equilibrium Fréedericksz distortions. Near a resulting multicritical bifurcation point a splay-roll instability and a bistability between the convective and the homogeneous states occur.

DOI: 10.1103/PhysRevE.67.031707 PACS number(s): 61.30.Gd, 47.54.+r, 47.20.Lz, 89.75.Kd

I. INTRODUCTION

Electroconvection (EC) in nematic liquid crystals (nematics) is widely accepted as an excellent paradigm to study pattern forming instabilities in anisotropic systems [1–5]. Nematics are intrinsically anisotropic fluids with uniaxial symmetry. The preferred axis (the director **n**) corresponds to the mean orientation of their elongated molecules. The EC occurs when a voltage above a critical threshold strength is applied across a thin layer of a nematic with nonvanishing electrical conductivity, which originates from impurities or suitable doping. At the convection onset typically a periodic array of convection rolls (stripes) is observed, which are associated with periodic director distortions perpendicular to the roll axes in the layer plane.

Besides the nonequilibrium EC instabilities alternatively equilibrium phase transitions (''Fréedericksz transitions'') can be observed if electric (or magnetic) fields are applied to the uniformly oriented nematics [2]. The resulting homogeneous director distortions, i.e., without spatial variations in the plane, are minimizers of the orientational elasticity potential characteristic for nematics [6]. The interplay between the periodic pattern-forming and the homogeneous modes is reflected in phenomena such as ''abnormal'' rolls [7–10] or ''dendritic growth'' [11] which have no counterpart in the standard Rayleigh-Bénard convection. The bifurcation diagrams are organized by various multicritical points mainly in the nonlinear regime, such that the theoretical analysis as well as the experimental verification are quite demanding. In the present case, the EC is discussed in a system, where equilibrium and nonequilibrium phase transitions and their competition are disentangled in a transparent manner, since a certain multicriticality is already seeded in the linear regime.

Our investigations concentrate on the familiar *planar* EC. In the common capacitorlike configuration an ac voltage $V(t)=\sqrt{2}U\cos(\omega t)$ is applied in the z direction between two transparent plates (in the xy plane), which confine a nematic layer. By a suitable surface treatment of the plates the director is orientated in a preferred direction (along $\hat{\mathbf{x}}$) in the layer plane. The effective voltage amplitude U and the circular ac frequency ω serve as main control parameters. All material properties of nematics require a tensorial description. For instance, the dielectricity tensor $\boldsymbol{\epsilon}$, which expresses the electric displacement $\mathbf{D}=\boldsymbol{\epsilon}\cdot\boldsymbol{\epsilon}_0\mathbf{E}$ in terms of the electric field $\mathbf{E}$, has the representation $\epsilon_{ij}=\epsilon_\perp\delta_{ij}+(\epsilon_\parallel-\epsilon_\perp)n_in_j$ $(i,j=x,y,z)$, which reflects the uniaxial symmetry. Obviously $\epsilon_\perp$ describes the dielectric response if $\mathbf{E}$ is oriented perpendicular to $\mathbf{n}$ while $\epsilon_\parallel$ governs the case $\mathbf{E}\|\mathbf{n}$. For positive dielectric anisotropy $\epsilon_a=\epsilon_\parallel-\epsilon_\perp>0$, the orientation of $\mathbf{n}$ parallel to $\mathbf{E}$ is energetically favored.

Historically, standard nematics, like 4-methoxy benzylidene-4′-n-butylaniline (MBBA) or a mixture, Merck Phase 5, with negative dielectric anisotropy ϵ_a have played a major role in the investigation of EC, since there was hope to exploit them for designing liquid crystal displays [12]. For this reason most of the material parameters for those substances have been measured, which has allowed a quantitative comparison with the theoretical calculations on the EC [13]. For instance, a spontaneously excited homogeneous *twist* mode, which corresponds to a rotation of the director in the plane of the nematic layer, has turned out to be essential for the interpretation of secondary instabilities in the planar EC [14,15]. A reverse sequence of bifurcations is typical for the *homeotropic* geometry (director orientation perpendicular to the confining plates, i.e., parallel to the applied electric field). First a primary Fréedericksz transition takes place leading virtually about the center plane of the cell to a planar configuration, which at increasing voltages becomes convectionally unstable via a secondary bifurcation [16].

In this paper we study *planar* EC in nematics with *positive* dielectric anisotropy $\epsilon_a>0$. This case, which has not attracted much interest so far, is in fact very convenient to investigate the competition between convective and homogeneous modes. While in the standard planar setup with $\epsilon_a<0$ the electric field $\mathbf{E}$ $(\|\hat{\mathbf{z}})$ is stabilizing, a destabilizing dielectric torque acts now on the director to align it with the field direction. However, an ensuing homogeneous distortion (the Fréedericksz transition) occurs only for an applied voltage amplitude U above a certain ω independent threshold $U_F=\pi\sqrt{k_{11}/(\epsilon_a\epsilon_0)}$ (see, e.g., [17], k_{11} denotes the splay elastic constant), since opposing torques from the orientational elasticity have to be overcome. The Fréedericksz transition can compete with the nonequilibrium EC instability of the basic state. The EC becomes possible above a frequency dependent threshold voltage $U_c(\omega)$, which increases monotonously with ω starting from $U_c(0)\approx\pi^2\sqrt{k_{11}\sigma_\perp/(\sigma_a\epsilon_\perp\epsilon_0)}$. The material constants $\sigma_\perp$ and σ_a are defined in analogy to $\epsilon_\perp$ and ϵ_a via the components of

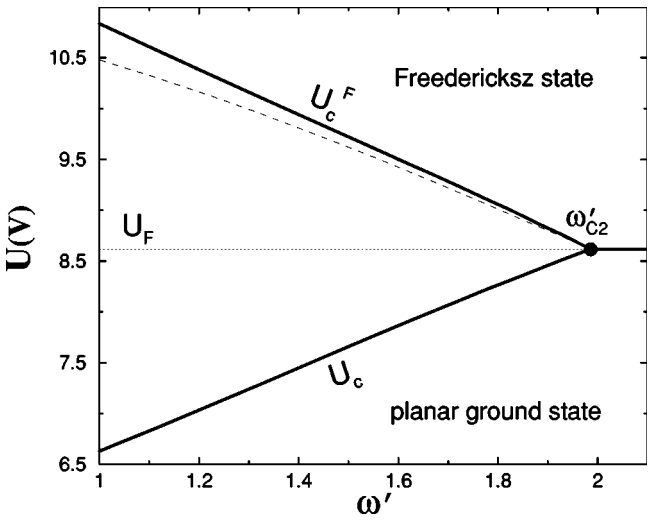

FIG. 1. Upper and lower convection onsets U_c, U_c^F as function of the dimensionless frequency $\omega' = \omega\tau_q$ together with the Fréedericksz bifurcation line $U_F = \pi\sqrt{k_{11}/(\epsilon_a\epsilon_0)}$ (solid lines) for MBBA* with $\epsilon_a = 0.1$. The dashed line indicates a weakly nonlinear approximation for U_c^F near the codimension-2 point ω'_{C2} (see Sec. III B below).

the conductivity tensor $\boldsymbol{\sigma} \equiv \sigma_{ij} = \sigma_\perp \delta_{ij} + \sigma_a n_i n_j$. Note that the ratio of $\epsilon_\perp$ and $\sigma_\perp$ defines the charge relaxation time $\tau_q = (\epsilon_\perp \epsilon_0)/\sigma_\perp$, which serves as a time scale in the sequel.

Inspection of the expressions for U_F and $U_c(0)$ above reveals that the Fréedericksz transition is, in fact, easily preempted by a primary EC instability at small ω and at not too large ϵ_a. With the increasing frequency $U_c(\omega)$ approaches U_F from below until the curves cross at a codimension-2 (C2) point $\omega = \omega_{C2}$. The experimental studies of nematics with positive ϵ_a have, in fact, exclusively concentrated on the *linear* threshold lines U_c, U_F, and the identification of ω_{C2} (see, e.g., [18,19] and further references therein). Materials for a wider range of positive dielectric anisotropies $\epsilon_a > 0$ were systematically synthesized by mixing MBBA with few weight percentages of suitable nematics (EBCA, MBCA) with large $\epsilon_a \approx 20$. Most material parameters (in particular the viscosities, see Sec. II below), which are needed for a precise comparison with the linear theory, have not been measured in these mixtures. However, the experimental U_c, U_F threshold values compared well with the theoretical calculations [18,19] on the basis of a material parameter set, to which we refer as MBBA* henceforth. In MBBA* except ϵ_a the material parameters of pure MBBA are used [20,21]. The explicit bifurcation diagrams presented in this paper are calculated for MBBA* with a representative medium value $\epsilon_a = 0.1$.

A simple consideration reveals that besides U_c, U_F a further instability line in the nonlinear regime has to meet the C2 point. If the voltage amplitude U is lowered starting in the Fréedericksz state for $U \gg U_F$ and for $\omega < \omega_{C2}$, one will hit for continuity reasons an upper transition line $U_c^F(\omega) > U_F > U_c(\omega)$ to the convection state. All the transition lines are sketched in Fig. 1 to underline from the beginning the generic framework for the bifurcation structure near ω_{C2}, which is detailed below. A comprehensive analysis of the bifurcation diagram in the vicinity of ω_{C2} has also revealed a rich variety of nonlinear bifurcation types. As an example for the complex structure of the multicritical point ω_{C2} it will be demonstrated below that the bifurcation at the lines U_c, U_F is supercritical, while it is subcritical and hysteretic at U_c^F. The resulting possibility of bistability between the convection states and the homogeneous Fréedericksz distortions has not been mentioned to our knowledge in the literature so far and might apply to other EC experiments as well.

The paper is organized as follows. In Sec. II we briefly present the fundamental equations as the basis of our theoretical calculations and define our notations. Section III contains the analysis of the convection onset at the bifurcation lines U_c and U_c^F. In Sec. IV the nonlinear bifurcation diagram for the substance MBBA* is presented and discussed in detail. With some concluding remarks the paper will end in Sec. V.

II. BASIC EQUATIONS

To explain the EC destabilization mechanism that has been elucidated first by Carr and Helfrich [22,23], a brief sketch of the standard nematohydrodynamic equations is sufficient [4,24]. They describe the coupling between the director **n**, the velocity **v**, and the electric field **E**, which derives as $\mathbf{E} = -\nabla\phi$ from the electric potential ϕ.

The important point is that in the presence of director distortions an electric current density $\mathbf{j}_e = \nabla\cdot(\boldsymbol{\sigma}\cdot\mathbf{E})$ is inevitably associated with a charge density $\rho_e = \nabla\cdot(\boldsymbol{\epsilon}\cdot\epsilon_0\mathbf{E})$ according to the continuity equation

$$\frac{d}{dt}\rho_e + \boldsymbol{\nabla}\cdot\mathbf{j}_e = 0, \tag{1}$$

with $d/dt = \partial_t + \mathbf{v}\cdot\boldsymbol{\nabla}$ the substantial derivative. The bulk force $\rho_e\mathbf{E}$ in the Navier-Stokes equation

$$\rho_m \frac{d}{dt}\mathbf{v} = \rho_e\mathbf{E} - \nabla p + \nabla\cdot\boldsymbol{\Sigma}, \tag{2}$$

with the pressure p and the mass density ρ_m, may then overcome the viscous stresses, to drive the velocity **v**. The fluid is assumed incompressible ($\boldsymbol{\nabla}\cdot\mathbf{v} = 0$). $\boldsymbol{\Sigma}$ denotes the stress tensor with viscous and (almost negligible) elastic contributions. The explicit form of $\boldsymbol{\Sigma}$ (see, e.g., [2,4]), which goes up to quintic order in the components of **v** and **n**, includes six (five independent) Leslie shear viscosity coefficients $\alpha_1, \ldots, \alpha_6$ [25]. The familiar effective (Miesowicz) viscosities that are determined by the relative orientations of **n** and **v** and the gradients of **v** depend linearly on α_i. For instance, the large shears $\partial_x v_z$ and $\partial_z v_x$ at a convection roll center in the planar case give rise to the Miesowicz viscosities $\eta_1 = (\alpha_4 + \alpha_5 - \alpha_2)/2$ and $\eta_2 = (\alpha_3 + \alpha_4 + \alpha_6)/2 < \eta_1$, respectively.

Eventually the director dynamics is governed by

$$\gamma_1 \mathbf{n}\times\frac{d}{dt}\mathbf{n} = \mathbf{n}\times(\mathbf{h}_{el} + \mathbf{h}_e + \mathbf{h}_v), \tag{3}$$

with $\gamma_1=\alpha_3-\alpha_2$. The restoring angular momenta in case of splay (k_{11}), twist (k_{22}), and bend (k_{33}) director distortions are contained in the effective field $\mathbf{h}_{el}$ derived from the Frank orientational elastic energy (see, e.g., [2,4,6]). The dielectric and viscous torques $\mathbf{h}_e$ and $\mathbf{h}_v$, respectively, are defined as

$$\mathbf{h}_e=\epsilon_a\epsilon_0(\mathbf{n}\cdot\mathbf{E})\mathbf{E}, \quad \mathbf{h}_v=-\alpha_2\mathbf{D}\cdot\mathbf{n}-\alpha_3\mathbf{n}\cdot\mathbf{D}, \tag{4}$$

where the tensor $\mathbf{D}(D_{ij}=\partial v_i/\partial x_j)$ characterizes the velocity shear. For example, the viscous torque contribution $-\alpha_2\partial_x v_z$ enhances the splay distortion of the director at the roll center. Equations (1)–(3) have to be solved with the rigid boundary conditions $\mathbf{v}=0$, $\mathbf{n}=\hat{\mathbf{x}}$ and $\phi=\phi_0=\mp\sqrt{2}U\cos(\omega t)$ at $z=\pm d/2$, with d the cell thickness.

For a more compact notation we combine in the following all field variables in a symbolic vector $\mathbf{V}=(\phi,\mathbf{n},\mathbf{v})$, so that the set of Eqs. (1)–(3) can be written in the symbolic form

$$\mathbf{B}\cdot\partial_t\mathbf{V}=\mathbf{L}\cdot\mathbf{V}+\mathbf{N}_2(\mathbf{V},\mathbf{V})+\mathbf{N}_3(\mathbf{V},\mathbf{V},\mathbf{V})+\cdots. \tag{5}$$

The components of the vector operators $\mathbf{N}_2$, $\mathbf{N}_3$, ... are quadratic, cubic, ... in $\mathbf{V}$ and its spatial derivatives, whereas $\mathbf{L}$ and $\mathbf{B}$ represent matrix differential operators.

III. ONSET OF CONVECTION

In the following the ''lower'' threshold curve U_c for the destabilization of the conductive ground state and the corresponding ''upper'' one, U_c^F, for the destabilization of the Fréedericksz state, already shown in Fig. 1, are analyzed in detail.

A. Lower onset of convection at U_c

The calculation of the lower onset of convection $U_c(\omega)$ requires a linear stability analysis of the planar ground state $\mathbf{V}_0=(\phi_0,\mathbf{n}_0,\mathbf{v}=0)$ with $\mathbf{n}_0=\hat{\mathbf{x}}$. From Eq. (5) we arrive by linearization of $\mathbf{V}=\mathbf{V}_0+\delta\mathbf{V}$ with respect to the convective perturbation $\delta\mathbf{V}(\mathbf{r},z,t)$ at the linear eigenvalue problem: $\mathbf{B}\cdot\partial_t\delta\mathbf{V}=\mathbf{L}\cdot\delta\mathbf{V}$. It is diagonalized by the ansatz $\delta\mathbf{V}(\mathbf{r},z,t)=e^{\lambda t}e^{i\mathbf{q}\cdot\mathbf{r}}\mathbf{V}(\mathbf{q},z)$ with $\mathbf{q}=(q,p)$. The eigenvalue $\lambda=\sigma+i\Omega$ with the maximal real part determines the growth rate $\sigma(\mathbf{q},\omega,U)$. The condition $\sigma=0$ yields the neutral curve $U_0(\mathbf{q},\omega)$ with the minimum $U_c(\omega)=U_0(\mathbf{q}_c,\omega)$ at $\mathbf{q}=\mathbf{q}_c(\omega)$. In the present case the bifurcation is stationary ($\Omega=0$) and we find typically normal rolls at threshold, i.e., $\mathbf{q}_c=q_c\hat{\mathbf{x}}$. Technically the eigenvalue problem is solved by a Galerkin method, where all fields are expanded with respect to the vertical coordinate z into a set of functions, that fulfill the (rigid) boundary conditions at the confining plates. The periodic time dependence of the eigenvector due to the applied ac voltage is captured by the Fourier series in time. The series expansions are appropriately truncated, such that the eigenvalue problem amounts to the diagonalization of a matrix acting in the space of the expansion coefficients. It turns out that the neutral curve is already very well described by keeping only the leading modes in z and t. One arrives thus at an one-mode approximation, that represents the dependence of the neutral curve on the material parameters in a particularly transparent manner,

$$U_0^2(q',\omega')=\frac{\pi^2 k_{11}}{\epsilon_\perp\epsilon_0}\frac{K(q')H(q',\omega')}{q'^2A(q')+(\epsilon_a/\epsilon_\perp)B(q',\omega')}. \tag{6}$$

In Eq. (6) the notations

$$K(q')=\frac{1+(k_{33}/k_{11})q'^2+(H_x/H_F)^2}{1+q'^2},$$

$$H(q',\omega')=\sigma(q')^2+\omega'^2\epsilon(q')^2,$$

$$\sigma(q')=q'^2(1+\sigma_a/\sigma_\perp)+1, \quad \epsilon(q')=q'^2(1+\epsilon_a/\epsilon_\perp)+1,$$

$$A(q')=\frac{a(q')}{\eta(q')}\equiv\frac{(\alpha_2q'^2-\alpha_3)\sigma(q')(\epsilon_a/\epsilon_\perp-\sigma_a/\sigma_\perp)}{\eta_2\lambda_1^4+(\alpha_1+\eta_1+\eta_2)\,i_1q'^2+\eta_1q'^4}I_h,$$

$$B(q',\omega')=\sigma(q')+\omega'^2\epsilon(q')$$

are used. The numerical constants $\lambda_1=1.505\,63$, $i_1=1.246\,52$, $I_h=0.972\,67$ correspond to certain overlap integrals, $q'=qd/\pi$ is the dimensionless wave number, and $\omega'=\omega\tau_q$ is the ac frequency in units of the charge relaxation time τ_q [26]. For convenience we have included the effect of a planar stabilizing magnetic field $\mathbf{H}=H_x\hat{\mathbf{x}}$, which is nondimensionalized in Eq. (6) with the help of the splay Fréedericksz field $H_F=(\pi/d)\sqrt{k_{11}/(\mu_0\chi_a)}$, $\chi_a>0$ denotes the anisotropy of the magnetic susceptibility. According to the representative example of Fig. 2(a) for MBBA* with $\epsilon_a=0.1$ the rigorous behavior of the critical voltage $U_c(\omega')=\min_{q'}U_0(q',\omega')$ is already determined very satisfactorily from Eq. (6). The lines U_c and U_F cross in this case at the C2 point, $\omega'_{C2}=1.99$.

The ω dependence of the critical wave number $q_c(\omega)$, which in fact slightly decreases with increasing ω' in Fig. 2(b), might look unexpected, since for $\epsilon_a<0$ we are accustomed to a monotonous increase of $q'_c(\omega')$ and a divergence also of U_c at the cutoff frequency ω'_{cut} (≈ 2 for MBBA with $\epsilon_a=-0.53$ [4]). The rather smooth variations of U_c, q_c with ω can be understood by examining more closely the threshold formula Eq. (6). Stabilizing mechanism are captured via the orientational elasticity term $K(q')>0$ and the viscous damping $\eta(q')>0$. The $a(q')$ term represents the essence of the Carr-Helfrich destabilizing mechanism: The factor $(\epsilon_a/\epsilon_\perp-\sigma_a/\sigma_\perp)<0$ displays the charge separation effect coupled to the hydrodynamic torque contribution $(\alpha_2q'^2-\alpha_3)<0$. The crucial difference in the threshold behavior between the standard MBBA and the MBBA* with $\epsilon_a>0$ comes from the dielectric torque term $(\epsilon_a/\epsilon_\perp)B(q')$, which is only weakly frequency dependent. For $\epsilon_a<0$ this term is negative (stabilizing) with a minimum at $q'=0$. The term $q'^2A(q')$, which has to compensate $(\epsilon_a/\epsilon_\perp)B(q')$ ($U_0^2>0$ is necessary for EC), has a maximum for $q'\sim 1.2$ for small frequencies that decreases with increasing ω' and shifts to larger q'. Since minimization of $U_0(q')$ requires, loosely speaking, maximization of the denominator in Eq. (6) the

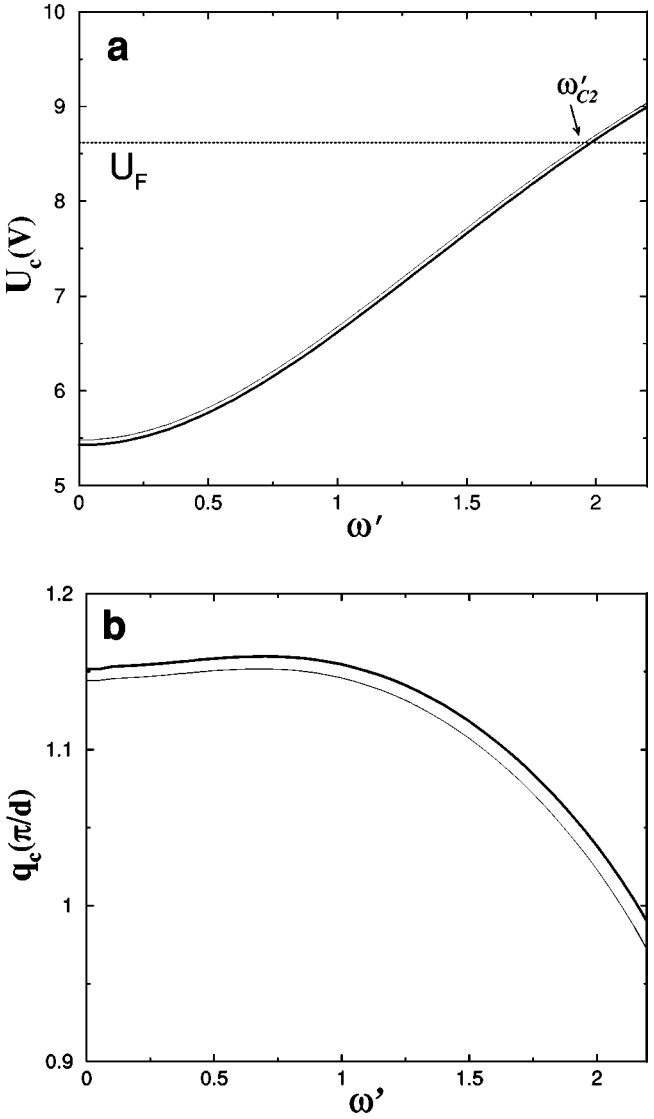

FIG. 2. Threshold voltage U_c (a) and critical wave number q_c in units of π/d (b) as function of the dimensionless frequency ω' for MBBA* with $\epsilon_a=0.1$ in comparison between rigorous numerical results (thick lines) and the analytical one-mode formula (6) (thin lines). The Fréedericksz threshold $U_F=\pi\sqrt{k_{11}/(\epsilon_a\epsilon_0)}$ is shown as well (a).

decrease of $A(q')$ with increasing ω' has to be balanced by larger q'_c values. In contrast, for $\epsilon_a>0$ the situation is just opposite, the contributions of $q'^2A(q')$ and $(\epsilon_a/\epsilon_\perp)B(q')$ add up, and $q'_c(\omega')$ will in fact even decrease.

With the use of Eq. (6) the linear properties of electroconvection can be easily assessed for other material parameters as well. For instance, the Fréedericksz transition U_F would precede U_c for $\epsilon_a\gtrsim 0.295$ for MBBA* as already mentioned in Ref. [4]. In general, one has also to be aware of a possible bifurcation to oblique rolls with the critical wave vector $\mathbf{q}_c=(q_c,p_c)$ including a finite angle with the preferred direction $\hat{\mathbf{x}}$ in the cell [4]. In this case the exact threshold behavior can also be described very well by a slightly more complicated one-mode formula [4,13], which contains Eq. (6) as a special case for $p_c=0$. While the threshold voltage in the case of an oblique roll bifurcation is only slightly below the normal roll threshold according to Eq. (6) the roll angle $\alpha=\arctan(p_c/q_c)$ is fairly sensitive against variations of the material parameters [4]. Finally we would like to mention that the convection regime can be enlarged with the use of an horizontal magnetic field [27]. The Fréedericksz threshold according to $U_F=\pi\sqrt{k_{11}/(\epsilon_0\epsilon_a)}\sqrt{1+(H_x/H_F)^2}$ is then shifted to larger values, whereas U_c reacts less sensitively. For instance, in the case of MBBA* with $\epsilon_a=0.1$ and for $H_x=H_F$ we find the values $U_F=12.19V$, $U(0)=6.26V$, such that the C2 point is shifted to the larger value, $\omega'_{C2}=3.06$ [cf. Fig. 2(a)].

B. Upper onset of convection at U_c^F

To calculate the upper onset of convection U_c^F a linear stability analysis of the Fréedericksz ground state $\mathbf{V}_F=(\phi,\mathbf{n}_F,\mathbf{v}=0)$ for $U>U_F$ has been performed starting from Eq. (5) with the use of the Galerkin methods.

It has turned out that the general behavior of U_c^F for $\omega'\lesssim\omega'_{C2}$ can be satisfactorily described by an analytical approach, where only the leading Galerkin coefficients are kept. The Fréedericksz solution that bifurcates supercritically at $U=U_F$ is calculated within a standard weakly nonlinear scheme. Near threshold the director reads $\mathbf{n}_F=(1,0,\psi_F\cos(\pi z/d))$ in the leading order of the amplitude ψ_F, which vanishes at U_F. To the order $O(\psi_F^3)$, where the corrections $\sim\psi_F^2$ to $n_x=1$ and ϕ_0 come into play, one arrives at a Landau-type equation $\partial_t\psi_F=\sigma_S\psi_F-g_F\psi_F^3$ with the saturation coefficient g_F and the splay growth rate

$$\sigma_S=\tau_d\frac{\epsilon_a\epsilon_0(U^2-U_F^2)}{\gamma_1 d^2}. \tag{7}$$

The linear growth rate σ_S crosses zero at U_F; $\tau_d=\alpha_0 d^2/(k_0\pi^2)$ denotes the director relaxation time, where $\alpha_0=10^{-3}$ N s/m^2 and $k_0=10^{-12}N$ set the scales for the viscosity and elasticity effects, respectively.

The calculation of g_F is straightforward and the final expression for g_F^{-1} can be read off in the square brackets of the following explicit representation:

$$\psi_F^2=\sigma_S\left[\frac{2\gamma_1 d^2}{\tau_d\pi^2\left(k_{33}-\frac{3}{4}k_{11}+C(U,\omega')\right)}\right]\equiv c_1[U^2-(U_F)^2], \tag{8}$$

$$C(U,\omega')=\frac{U^2\epsilon_a\epsilon_0}{\pi^2}\left(\frac{3}{4}+\frac{\sigma_a/\sigma_\perp+\omega'^2\epsilon_a/\epsilon_\perp}{1+\omega'^2}\right),$$

which is valid in the limit $U\to U_F$, $\omega'\to\omega'_{C2}$.

In the next step the linear stability analysis of the Fréedericksz solution has to be performed. For finite ψ_F the planar director symmetry is broken and the periodic director fluctuation crucial in the Helfrich mechanism to drive EC are impeded; consequently, the threshold must increase compared to U_c. Technically one has to repeat the calculations

that led to U_c [see Eq. (6)], but now for the nontrivial distorted ground state ($\mathbf{n}=\mathbf{n}_F$). We will skip the straightforward though somewhat lengthy calculations. The final result in the vicinity of ω'_{C2} becomes very transparent if written in the following form: $(U_c^F)^2-(U_c)^2=c[(U_c^F)^2-(U_F)^2]\propto\psi_F^2$, consistent with $U_c^F=U_c$ at $\psi_F=0$. Solving for U_c^F we obtain

$$(U_c^F)^2=\frac{c(U_F)^2-(U_c)^2}{c-1}, \quad c=c_1c_2 \quad (c>1). \tag{9}$$

It turns out that the factor c_2, which has to be calculated numerically, depends mainly on some overlap integrals, while the material parameter dependence is condensed in the parameter c_1 defined in Eq. (8). It is obvious from Eq. (9) that the line U_c^F starts at the C2 point ($U_c=U_F$) as well. Furthermore, inspection of Eq. (8) proves that for fixed ϵ_a, σ_a an increase of the bend constant k_{33} leads to a decrease of ψ_F and c_1. Thus the slope of $U_c^F(\omega')$ depends rather sensitively on k_{33}, which is, for instance, known to increase strongly with temperature near a nematic-smectic transition [28]. In Fig. 1 the analytical threshold curve U_c^F with $c_1\approx 0.019$, $c_2\approx 97.8$ for MBBA* ($\epsilon_a=0.1$) is compared with the rigorous numerical results. As to be expected from our weakly nonlinear approach there is, in fact, a good agreement near the C2 point ω'_{C2} where ψ_F is not too large.

IV. NONLINEAR REGIME

After the discussion of the linear threshold lines U_c, U_F, and U_c^F in Sec. III we will now turn to the phase diagram for the nonlinear states that bifurcate at these lines. Our numerically demanding analysis has focused on the interesting regime near $\omega'=\omega'_{C2}$, since for lower frequencies the well-investigated familiar EC bifurcation scenarios for $\epsilon_a<0$ (see, e.g., [24]) were expected and indeed found in some selected test runs (for more details see [29]). The analysis of the periodic solutions and their stability is again based on Galerkin methods, by which Eq. (5) is mapped on a system of nonlinear algebraic equations for the expansion coefficients with respect to suitable test functions. The equations are solved by a Newton iteration scheme and, in general, tested for stability with the use of the standard methods [13,24].

In Fig. 3 the complete phase diagram in the U,-ω' plane near the C2 point ($\omega'_{C2}=1.99$) is shown, which is considered to be generic for the EC instabilities in nematics with slightly positive ϵ_a. Let us discuss at first the white wedged-shaped convection regime delineated by the lines U_c and U_c^F. Increasing the applied voltage at lower ω' the normal rolls above U_c become at first unstable against the long-wavelength zigzag (ZZ) instability, which involves undulations along the roll axis. At the line U_S, on the other hand, a homogeneous splay mode $n_z^S=\psi_S\cos(\pi z/d)$ spontaneously bifurcates. For ω' larger than the crossing point, $\omega'=1.75$, of U_{ZZ} and U_S, the splay mode is directly superimposed onto the periodic director distortion with amplitude A leading to the so-called splay rolls [15] characterized by the off-plane director component $n_z=[A\cos(qx)+\psi_S]\cos(\pi z/d)$. The bifurcation at U_S in Fig. 3 is supercritical and can appear

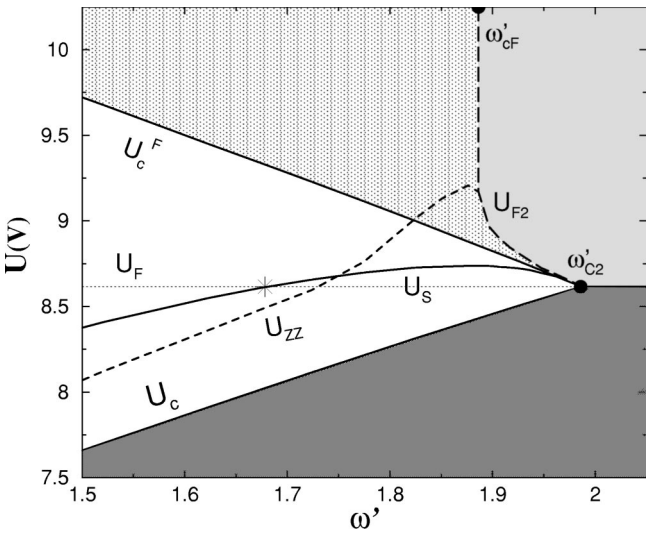

FIG. 3. Complete phase diagram for MBBA* with $\epsilon_a=0.1$ for frequencies ω' near the C2 point ω'_{C2} (see text) on the basis of the Galerkin calculations for rolls with the critical wave vector $q_c(\omega')$. The bifurcation lines above onset (U_c) indicate the zigzag instability (U_{ZZ}), the Fréedericksz transition (U_F), the splay-roll bifurcation (U_S), the Fréedericksz → convection (U_c^F), and the convection → Fréedericksz transition (U_{F2}).

above or below the (in the convection regime, $\omega'<\omega'_{C2}$, irrelevant) line U_F. Although the transition is certainly favored by the dielectric torque for $\epsilon_a>0$, it is also driven by complex nonlinear interactions between the director and the flow field. In fact, splay rolls have been identified and discussed also in buoyancy driven thermal convection in nematics [15].

The interaction between the convection-mode amplitude A and the homogeneous splay director distortion ψ_S is captured by the coupled order parameter equations for A and ψ_S:

$$\begin{aligned}\partial_t A&=(\sigma_R-g_R|A|^2-\beta\psi_S^2)A,\\ \partial_t\psi_S&=(\sigma_S+\Gamma_\psi|A|^2)\psi_S.\end{aligned} \tag{10}$$

All coefficients have been calculated and a good agreement with the Galerkin analysis has been found. For $\psi_S=0$ the A equation describes the supercritical bifurcation of the rolls with the amplitude $A^2=\sigma_R/g_R\propto U^2/U_c^2-1$ at U_c. The splay-roll bifurcation takes place, when the effective growth rate $\sigma_S^{eff}=\sigma_S+\Gamma_\psi A^2$ becomes larger than zero. The coefficient Γ_ψ is negative for smaller ω' before it changes sign at $\omega'<\omega'_S=1.68$, marked by a star in Fig. 3. The form of $U_S(\omega')$ can be understood on the basis of Eq. (10): In the regime $\omega'<\omega'_S$ a splay bifurcation at $U_S<U_F$ is possible, because the contribution $\Gamma_\psi A^2>0$ in σ_S^{eff} can compensate σ_S, which is negative for $U<U_F$ [cf. Eq. (7)]. For $\omega'>\omega'_S$ the negative Γ_ψ term suppresses at first the positive σ_S term in σ_S^{eff} resulting in $U_S>U_F$.

Of particular interest is the upper bifurcation line U_c^F [see also Eq. (9) and Fig. 1], at which the Fréedericksz state becomes convectionally unstable when *lowering* the voltage

from above. A weak nonlinear expansion slightly above the line U_c^F with respect to the convective perturbation yields a negative saturation coefficient g for frequencies $\omega' < \omega'_{C2}$ in the resulting Landau equation, indicating a subcritical bifurcation. g is strongly decreasing with frequency, i.e., the subcritical nature becomes more pronounced at lower ω'. However, it should be emphasized that line U_c^F has in principle no relevance, when the voltage is *increased* from below, i.e., when starting from convective Galerkin solutions inside the white wedged-shaped regime in Fig. 3. In fact, we found these solutions to exist far beyond U_c^F in the nonlinear regime, but we were not able to study systematically their stability. Only in an intermediate frequency range $\omega'_{cF} < \omega' < \omega'_{C2}$ above (and on the right of) the line U_{F2} in Fig. 3 convection ceased to exist. Thus, in contrast to the unique Fréedericksz-solution in the bright gray region, *bistability* exists between the Fréedericksz and convective solutions in the gray-shaded area enclosed between U_c^F and U_{F2}.

For a better illustration of the subcritical nature of the convection onset at U_c^F and the interplay between the Fréedericksz state and the convection, it is useful to follow the order parameters A and ψ (obtained as the Galerkin solutions), when the reduced control parameter $\epsilon = U^2/U_c^2 - 1$ is continuously increased at fixed ω'. The case $\omega' = 1.88$ slightly below $\omega'_{cF} = 1.89$ is shown in Fig. 4(a). At first the amplitude A (solid line) of the periodic roll state grows $\propto \sqrt{\epsilon}$ above $\epsilon = 0$ in line with the supercritical bifurcation at U_c. At ϵ_S the homogeneous splay mode ψ_S (dot-dashed line) bifurcates. Though a further increase in A is then slowed down, splay-roll convection solution continue to exist up to large ϵ, as already mentioned. On the other hand, we have learnt from our previous considerations in Sec. III, that a pure Fréedericksz state ψ_F with $A = 0$, which bifurcates at ϵ_F, can exist only for $\epsilon > \epsilon_c^F = (U_c^F)^2/U_c^2 - 1$ (thick dashed line). Thus, decreasing ϵ in the Fréedericksz state from above leads in any case at $\epsilon = \epsilon_c^F$ to a discontinuous jump [indicated by the double arrows in Fig. 4(a)] from the Fréedericksz solution $n_z^F = \psi_F \cos(\pi z/d)$ [Eq. (8)] to the splay rolls [Eq. (10)] with $A, \psi_S \neq 0$. Obviously, for $\epsilon > \epsilon_c^F$ we recover the bistability between the convection and the Fréedericksz state.

The situation changes for frequencies $\omega' > \omega'_{cF}$ since the bistable regime is restricted to an ϵ range between ϵ_c^F and ϵ_{F2} in Fig. 4(b). Above $\epsilon_{F2} \simeq 0.105$ only the Fréedericksz solution exists ($A = 0$, $\psi = \psi_F$). As demonstrated in Fig. 4(b) the point $\epsilon = \epsilon_{F2}$ corresponds then to the saddle node (S) of the backward bifurcation at ϵ_c^F, which connects the stable and unstable branches of the roll- and splay mode A and ψ_S, respectively. At ϵ_c^F the splay amplitude branch ψ_S and the Fréedericksz solution ψ_F have to merge in line with Fig. 4(b). The upper solid A line in Fig. 4(b), which approaches zero at $\epsilon = 0$ (not shown) corresponds to the A line in Fig. 4(a). In the same manner ψ_F (dashed) approaches zero at ϵ_F, as shown in Fig. 4(a). When approaching ω'_{cF} from above, the saddle node moves obviously to large ϵ along the almost vertical separation line U_{F2} for $\omega' = \omega'_{cF}$ in Fig. 3. Note that the unstable solutions starting at ϵ_c^F in Fig. 4(b) have not vanished; only for clarity they are suppressed in Fig. 4(a), because they have no physical relevance.

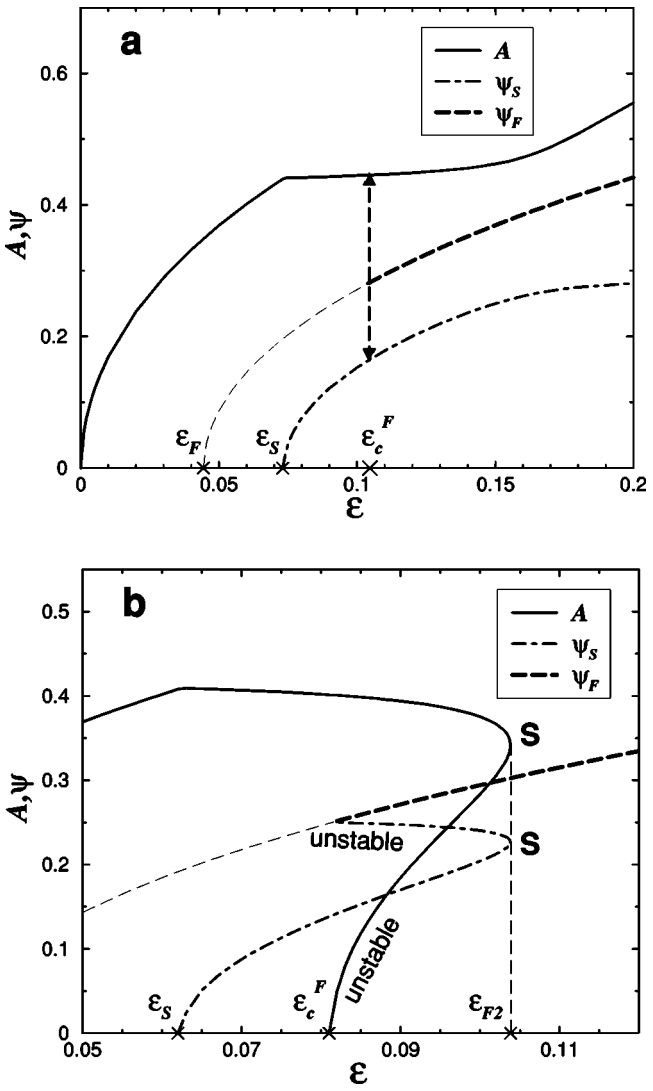

FIG. 4. Amplitudes for the off-plane director-distortion $n_z = [A\cos(q_c x) + \psi_S + \psi_F]\cos(\pi z/d)$ as function of the reduced control parameter $\epsilon = U^2/U_c^2 - 1$ for frequencies slightly below or above the transition frequency $\omega'_{cF} = 1.89$ at $\omega' = 1.88$ (a) and $\omega' = 1.90$ (b). A describes the periodic off-plane director excursions in convection rolls and ψ_S, ψ_F the homogeneous splay distortion in the convection or the Fréedericksz state, respectively. For a detailed explanation, see text.

V. CONCLUSION

In conclusion we have demonstrated that planar nematics with slightly positive ϵ_a (and positive σ_a) show interesting nonlinear EC states, which result from the competition between a convection mode and a homogeneous splay mode. Above the subcritical transition U_c^F from the Fréedericksz into convection state a bistability between a Fréedericksz solution (equilibrium state) and a convective solution (nonequilibrium state) was clearly identified. A transition frequency ω_{cF} could be determined below which we have been able to

construct splay-roll solutions up to high voltages, whereas for $\omega > \omega_{cF}$ with increasing voltage a discontinuous transition to a Fréedericksz state occurs. The bifurcation diagrams are believed to display the generic features. Support stems from the detailed physical interpretation of the destabilization mechanism as well as from the observation that parameter modifications led only to some quantitative changes. We hope that our comprehensive theoretical analysis will motivate future experimental studies. Besides a careful exploration of the linear destabilization lines U_c, U_c^F, and the C2 point, the investigation of the bistable regime above U_c looks promising. One might, for instance, achieve a better insight into the nature of inhomogeneous Fréedericksz states in the presence of walls between symmetry degenerated configurations $\pm\psi_F$ where, according to Eq. (2), also a flow is excited.

ACKNOWLEDGMENTS

We would like to thank I. Rehberg, T. Bock, and L. Kramer for useful discussions.

[1] M.C. Cross and P.C. Hohenberg, Rev. Mod. Phys. **65**, 851 (1993).
[2] P.G. de Gennes, *The Physics of Liquid Crystals* (Clarendon Press, Oxford, 1974).
[3] S. Kai and W. Zimmermann, Prog. Theor. Phys. Suppl. **99**, 458 (1989).
[4] E. Bodenschatz, W. Zimmermann, and L. Kramer, J. Phys. (Paris) **49**, 1875 (1988).
[5] L. Kramer and W. Pesch, Annu. Rev. Fluid Mech. **27**, 515 (1995).
[6] F.C. Frank, Discuss. Faraday Soc. **25**, 19 (1958).
[7] H. Richter, A. Buka, and I. Rehberg, in *Spatio-Temporal Patterns in Nonequilibrium Complex Systems*, edited by P.E. Cladis and P. Palffy-Muhoray (Addison-Wesley, New York, 1995).
[8] J.-H. Huh, Y. Hidaka, and S. Kai, Phys. Rev. E **58**, 7355 (1998).
[9] W. Pesch and U. Behn, in *Evolution of Spontaneous Structures in Dissipative Continuous Systems*, edited by F.H. Busse and S.C. Müller (Springer, Berlin, 1998).
[10] L. Kramer, B. Dressel, H. Zhao, and W. Pesch, Mol. Cryst. Liq. Cryst. Sci. Technol., Sect. A **364**, 101 (2000).
[11] J.T. Gleeson, Nature (London) **256**, 511 (1996).
[12] See, e.g., G.H. Heilmeier, L.A. Zanoni, and L.A. Barton, Proc. IEEE **56**, 1162 (1968); B.J. Lechner, F.J. Marlowe, and E.O. Nester, *ibid.* **59**, 1566 (1971).
[13] L. Kramer and W. Pesch, in *Pattern Formation in Liquid Crystals*, edited by A. Buka and L. Kramer (Springer, New York, 1996).
[14] E. Plaut, W. Decker, A.G. Rossberg, L. Kramer, W. Pesch, A. Belaidi, and R. Ribotta, Phys. Rev. Lett. **79**, 2367 (1997).
[15] B. Dressel, A. Joets, L. Pastur, W. Pesch, E. Plaut, and R. Ribotta, Phys. Rev. Lett. **88**, 024503 (2002).
[16] H. Richter, N. Klöpper, A. Hertrich, and A. Buka, Europhys. Lett. **30**, 37 (1995).
[17] W.H. de Jeu, C.J. Gerritsma, and T. Lathouwers, Chem. Phys. Lett. **14**, 5031 (1972).
[18] M.I. Barnik, L.M. Blinov, M.F. Grebenki, S.A. Pikin, and V.G. Chigrinov, Phys. Lett. **51A**, 175 (1975).
[19] P.R. Kishore, Mol. Cryst. Liq. Cryst. **128**, 75 (1985); P.R. Kishore, T.F.S. Raj, A.W. Iqbal, S.S. Sastry, and G. Satyanandam, Liq. Cryst. **14**, 1319 (1993).
[20] The material parameter set MBBA I in Ref. [4] is used except that ϵ_a is allowed to vary. In line with [4] the average dielectric constant $\bar{\epsilon} = (2\epsilon_\perp + \epsilon_\parallel)/3$ is fixed for convenience to the pure MBBA value $\bar{\epsilon} = 5.07$.
[21] The molecular structure of large ϵ_a materials such as EBCA (4-ethoxybenzylidene-4′-cyanoaniline) differs mainly by substituting the butyl group in MBBA (4-methoxybenzylidene-4′-*n*-butylaniline) by the strongly polarizable cyano group. In the mixture MBBA-EBCA the resulting value ϵ_a varies linearly with the concentration of EBCA; for instance, $\epsilon_a = 0.1$ corresponds to a concentration of $\approx 2.3\%$ (weight percentage) [19]. Thus, it is not surprising that MBBA* with the material parameters of pure MBBA, except ϵ_a, describe well the experiments.
[22] E.F. Carr, Mol. Cryst. Liq. Cryst. **7**, 253 (1969).
[23] W. Helfrich, J. Chem. Phys. **51**, 4092 (1969).
[24] E. Plaut and W. Pesch, Phys. Rev. E **59**, 1747 (1998).
[25] F.M. Leslie, Q. J. Mech. Appl. Math. **19**, 357 (1966).
[26] Although depending on the choice of certain test functions previous one-mode formulas to be found in the literature [4,13] look slightly different, their results match practically with Eq. (6). Note that the threshold U_0 [Eq. (6)] depends only on the ratios of the viscosity coefficients $\alpha_i (i = 1, \ldots, 6)$, which fulfill the Parodi relation $\alpha_2 + \alpha_3 = \alpha_6 - \alpha_5$. According to the definition of the Miesowicz coefficients η_1, η_2 [see paragraph after Eq. (2)], only the sum $\alpha_4 + \alpha_5$ enters, such that in fact only *three* independent combinations of α_i are relevant. In addition, from the measurements of $U_F = \pi\sqrt{k_{11}(\epsilon_a \epsilon_0)}$, of the codimension-2 point ω_{C2} in units of $\tau_q = (\epsilon_\perp \epsilon_0)/\sigma_\perp$ and of $U_0(\omega)$, one gets further valuable informations to asses the parameters.
[27] The theoretical analysis in Ref. [19], based on an old analytical threshold formula [E. Dubois-Violette, P.G. de Gennes, and O. Parodi, J. Phys. (Paris) **32**, 305 (1971)], is only useful to reproduce qualitative trends in the dependence on the material parameters. In contrast to Eq. (6), one finds considerable quantitative deviations from the rigorous numerical results.
[28] F. Jähnig and F. Brochard, J. Phys. (Paris) **35**, 301 (1974).
[29] B. Dressel, Ph.D. thesis, Bayreuth, 2002 (unpublished).